ACS OMEGA

Open Access

http://pubs.acs.org/journal/acsodf

Article

Characteristics and Influence Factors of Natural Desorption in Coal Bodies from Fukang Mining Area, Xinjiang, China

Liang Du, Xuchao Huang, Zhengshuai Wang, Chuanjian Cheng, Kuwanixibieke Maimaitizhuma, Haichao Wang,* Zhenzhi Wang,* Zhiwei Zeng, Bing Luo, Mengmeng Yang, Zheyuan Ouyang, Wei Dou, Beixi Zhang, and Teng Li

Cite This: *ACS Omega* 2023, 8, 40417−40432

Read Online

ACCESS | Metrics & More | Article Recommendations

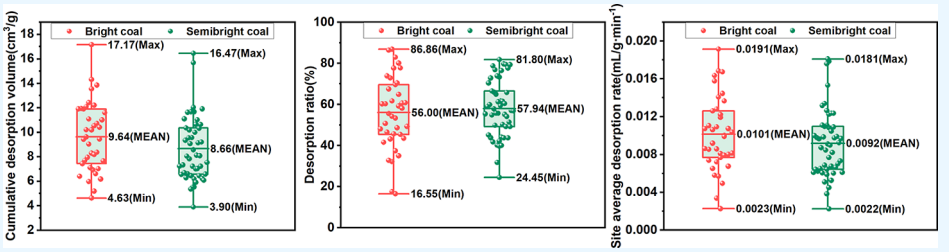

ABSTRACT: Coal body desorption characteristics are one of the key factors that influence the development of coalbed methane (CBM). In this study, 91 coal core samples from 11 CBM wells in the Fukang mining area were collected from Xinjiang, China, and the coal quality, high-pressure mercury compression, gas content, and natural desorption characteristics measurements were launched. With the detailed analyses of the differences in cumulative desorption volume, desorption ratio, and on-site average desorption rate for the coal samples with different body structures and macrolithotypes, the influence of the maximum reflectance of vitrinite, microscopic coal rock composition, and coal quality and pore characteristics on CBM desorption characteristics were discussed. The results showed that the cumulative desorption volume, desorption ratio, and desorption rate of cataclastic structure-bright coal are higher than those of primary structure-semibright coal. With the increase of $R_{O,max}$ and vitrinite content, the adsorption capacity of coal increases, and the increased methane concentration difference during desorption leads to an increase in cumulative desorption volume and on-site average desorption rate. The higher contents of moisture and ash yield would occupy the adsorption sites and hinder gas diffusion, which would decrease the desorption of coalbed methane. The greater porosity/pore volume ratio of medium and large pores can enhance the connectivity of pores, which increases the desorption ratio and the average desorption rate, while the higher micropore porosity/pore volume ratio can increase the gas adsorption space and the cumulative desorption volume. The pore characteristics have the most significant effect on the cumulative desorption volume and desorption ratio. The results of the study can help guide coal mine gas management and CBM development from middle-and low-rank coal reservoirs in Xinjiang.

1. INTRODUCTION

Coalbed methane (CBM) is mainly adsorbed on the surface of the coal matrix and pores in the coal,[1] and only small amounts of free CBM are stored in pores and fractures. In coal seams, adsorbed and free CBM exist in dynamic equilibrium. As a clean and high-quality energy source, the CBM well development and coal mine extraction are two dominant development methods in China. With the continuous discharge of water in the coal seams, the reservoir pressure is decreased,[2] the dynamic balance of the gas is broken in the coal seam, and the adsorbed CBM desorbs from the coal-matrix surface and pores, and the CBM diffuses into cracks and migrates to the extraction pipeline.[3] At different pore scales, gas migration follows Knudsen, Fick's, and transitional diffusion,[4] and the previous scholars have constructed various diffusion models to characterize and predict coal gas diffusion,[5−8] such as the unipore model, the bidisperse model, the triple-pore models, and the multiporous model, which could be utilized to describe the migration of gas molecules in pores. The reasonable desorption parameters could feature the gas migration characteristics in the coal seams, which could optimize the utilization of CBM development methods and predict the extraction cycle. Therefore, detailed study of the desorption

Received: July 9, 2023
Revised: September 13, 2023
Accepted: October 3, 2023
Published: October 20, 2023

Table 1. 91 Sample Parameters Table

coal sample	M_{ad} (%)	A_d (%)	coal rock type	coal mass structure	vitrinite content (%)	$R_{o,max}$ (%)	total desorption amount (cm^3/g)	gas content (cm^3/g)	lost gas content (cm^3/g)	total desorption volume in the first 8 h (cm^3/g)	desorption ratios (%)	on-site average desorption rate ($\times10^{-3}\cdot cm^3/g\cdot min^{-1}$)
CS13-1-A3-1	1.82	14.59	bright coal	cataclastic texture	98.8	0.72	4.63	5.58	0.95	4.63	82.95	7.66
FK2-A3-8	2.48	8.34	bright coal	cataclastic texture	98.8	0.54	5.97	6.73	0.75	4.68	69.57	8.10
CS13-1-A2-17	2.04	6.83	bright coal	cataclastic texture	96.8	0.73	10.19	11.69	1.50	7.21	61.71	11.90
CS16-X1-A2-17	1.86	3.9	bright coal	cataclastic texture	93.2	0.65	11.08	14.38	3.30	12.49	86.86	19.15
CS16-X1-A2-5	1.71	4.7	bright coal	cataclastic texture	96.9	0.6	13.55	15.55	2.00	10.08	64.82	16.83
CS8-X4-A2-7	2.24	7.55	bright coal	cataclastic texture	96.7	0.62	6.93	8.47	1.54	6.78	80.03	10.91
FC-2-39-3	1.63	11.65	bright coal	cataclastic texture	92.4	0.69	7.11	7.52	0.16	1.24	16.55	2.26
FC-2-41-1	1.63	9.12	bright coal	cataclastic texture	98.4	0.73	6.61	8.05	1.44	6.25	77.69	10.03
FK16-A3-1	1.38	14.6	bright coal	cataclastic texture	71.2	0.92	7.95	9.68	1.61	8.36	86.33	14.06
FK16-A5-2	1.41	3.17	bright coal	cataclastic texture	86.8	0.69	12.42	13.38	0.96	6.11	45.68	10.62
FK16-A5-4	1.4	3.64	bright coal	cataclastic texture	92.5	0.74	8.29	9.45	1.16	6.37	67.41	10.74
FK16-A5-6	1.28	7.94	bright coal	cataclastic texture	93.1	0.75	12.20	13.45	1.25	7.18	53.37	12.22
FK16-A7-1	1.51	8.29	bright coal	cataclastic texture	97.7	0.73	10.53	11.57	0.83	4.32	37.37	7.20
FK16-A7-2	1.49	4.95	bright coal	cataclastic texture	82.9	0.78	10.21	10.84	0.27	1.90	17.56	3.37
FK16-A9-1	1.6	2.24	bright coal	cataclastic texture	96	0.7	9.03	10.30	0.55	3.31	32.09	5.69
FK18-A3-1	1.65	4.01	bright coal	cataclastic texture	79.9	0.82	10.73	11.54	0.81	4.98	43.14	8.58
FK18-A3-2	1.62	11.88	bright coal	cataclastic texture	85.1	0.84	7.02	8.21	1.19	5.99	72.91	9.88
FK18-A5-1	1.5	5.1	bright coal	cataclastic texture	96.2	0.7	11.89	12.71	0.82	6.18	48.59	11.05
FK18-A5-2	1.39	12.07	bright coal	cataclastic texture	97.8	0.69	10.42	11.23	0.76	5.22	46.44	9.19
FK18-A5-6	1.4	4.6	bright coal	cataclastic texture	98.3	0.72	12.10	12.63	0.53	4.42	34.98	8.01
FK18-A5-7	1.48	2.74	bright coal	cataclastic texture	90.8	0.66	11.94	12.80	0.78	5.80	45.33	10.35
FK2-A3-11	2.44	3.81	bright coal	cataclastic texture	97.8	0.54	7.70	8.53	0.83	4.62	54.17	7.91
FK2-A3-7	2.25	12.42	bright coal	cataclastic texture	92.7	0.53	6.17	7.02	0.84	4.94	70.42	8.55
FK2-A3-9	2.47	4.65	bright coal	cataclastic texture	93	0.55	7.44	7.97	0.50	3.31	41.52	5.79
FS-24-39-1	1.65	8.93	bright coal	cataclastic texture	98.2	0.64	7.65	8.71	0.63	3.79	43.52	6.52
FS-24-39-3	1.76	8.9	bright coal	cataclastic texture	98.2	0.67	11.00	12.16	1.16	7.37	60.60	12.80
FS-24-39-5	1.6	4.8	bright coal	cataclastic texture	97.1	0.65	11.91	13.28	1.37	8.01	60.29	13.67
FS-24-40-3	1.44	2.79	bright coal	cataclastic texture	87.9	0.66	17.17	18.67	1.39	8.97	48.06	15.79
FS-24-41-8	1.18	16.48	bright coal	cataclastic texture	98.5	0.7	14.30	16.01	1.63	9.48	59.20	16.35
FS-24-42-9	1.29	3.18	bright coal	cataclastic texture	98.7	0.76	13.85	14.97	1.07	9.10	60.77	16.73
FS-24-43-1	1.47	3.49	bright coal	cataclastic texture	90.9	0.77	6.39	7.27	0.77	4.04	55.58	6.75
FS-24-43-2	1.26	12.01	bright coal	cataclastic texture	93.2	0.77	11.59	13.38	1.72	7.77	58.09	12.62
FS60-39[2]-1	1.39	4.28	bright coal	cataclastic texture	86.1	0.68	8.19	8.64	0.44	2.83	32.71	4.93
FC-2-41-4	1.14	49.66	bright coal	cataclastic texture	96.9	0.73	5.20	6.37	1.17	4.70	73.84	7.36

https://doi.org/10.1021/acsomega.3c04911
ACS Omega 2023, 8, 40417−40432

Table 1. continued

coal sample	M_{ad} (%)	A_d (%)	coal rock type	coal mass structure	vitrinite content (%)	$R_{o,max}$ (%)	total desorption amount (cm^3/g)	gas content (cm^3/g)	lost gas content (cm^3/g)	total desorption volume in the first 8 h (cm^3/g)	desorption ratios (%)	on-site average desorption rate ($\times10^{-3}\cdot cm^3/g\cdot min^{-1}$)
FC-2-41-5	2.03	9.05	bright coal	cataclastic texture	97.5	0.74	9.62	12.03	2.42	9.35	77.73	14.44
FS60-41-5	1.17	20.9	bright coal	cataclastic texture	97.1	0.74	8.37	9.07	0.66	4.60	50.77	8.13
FS60-41-7	1.47	8.84	bright coal	cataclastic texture	92.2	0.72	9.41	10.73	1.26	6.46	60.19	10.72
FS60-41-8	1.46	8.87	bright coal	cataclastic texture	94.7	0.73	9.45	10.44	0.96	5.14	49.25	8.62
CS13-1-A1-1	2.2	14.79	semibright coal	cataclastic texture	85.7	0.66	6.19	7.19	0.90	5.27	73.31	9.11
CS13-1-A2-5	1.94	6.45	semibright coal	cataclastic texture	95.2	0.6	8.58	10.37	1.78	7.66	73.84	12.24
CS13-1-A6-1	1.67	4.54	semibright coal	cataclastic texture	93.7	0.63	7.22	8.57	1.35	6.55	76.41	10.83
CS13-1-A7-1	1.6	1.63	semibright coal	cataclastic texture	87.7	0.64	5.53	6.34	0.81	4.87	76.78	8.45
CS13-1-A8-3	1.7	6.47	semibright coal	cataclastic texture	89.3	0.7	7.00	8.31	1.31	6.63	79.73	11.07
CS13-1-A8-7	1.73	9.22	semibright coal	cataclastic texture	95.4	0.72	6.46	7.86	1.41	6.43	81.80	10.46
CS16-X1-A4-1	2.16	8.28	semibright coal	cataclastic texture	99.2	0.59	11.68	14.70	3.01	11.58	78.80	17.86
CS8-X4-A2-1	2.19	4.75	semibright coal	cataclastic texture	89.2	0.61	9.58	10.86	1.19	6.45	59.39	10.96
FC-2-39-1	1.85	3.47	semibright coal	cataclastic texture	95.2	0.66	9.99	10.85	0.86	4.58	42.20	7.67
FC-2-39-2	2.13	4.56	semibright coal	cataclastic texture	95.3	0.7	9.08	9.94	0.86	3.99	40.13	6.44
FC-2-41-2	1.86	28.09	semibright coal	cataclastic texture	89.7	0.76	8.12	10.18	2.06	8.08	79.42	2.24
FC-2-41-3	0.71	76.09	semibright coal	cataclastic texture	87.5	0.72	3.90	4.58	0.68	2.83	61.71	4.48
FK16-A4-1	1.36	22.65	semibright coal	cataclastic texture	74.9	0.78	7.03	7.95	0.69	3.50	44.07	5.87
FK16-A5-1	1.35	7.24	semibright coal	cataclastic texture	97	0.78	11.75	13.17	1.21	7.33	55.69	12.63
FK16-A5-10	1.23	4.15	semibright coal	cataclastic texture	80.5	0.8	10.65	12.20	1.48	7.47	61.22	12.35
FK16-A5-3	1.42	3.84	semibright coal	cataclastic texture	86.6	0.75	11.68	12.74	1.06	6.34	49.79	10.89
FK16-A5-5	1.46	2.94	semibright coal	cataclastic texture	60.3	0.76	11.02	11.83	0.81	5.17	43.67	8.99
FK16-A5-7	1.35	11.17	semibright coal	cataclastic texture	96.7	0.76	10.18	11.43	0.96	5.73	50.16	9.84
FK16-A5-8	1.28	8.47	semibright coal	cataclastic texture	75.8	0.77	10.32	11.18	0.69	4.66	41.72	8.20
FK16-A5-9	1.37	2.81	semibright coal	cataclastic texture	85.7	0.79	11.63	12.27	0.64	4.87	39.71	8.72
FK16-A7-3	1.57	1.69	semibright coal	cataclastic texture	88.3	0.7	9.54	11.28	1.72	8.22	72.83	13.39
FK16-A7-4	1.42	14.07	semibright coal	cataclastic texture	61.7	0.77	7.82	9.48	1.44	7.36	77.66	12.35
FK16-A8-1	1.54	28.94	semibright coal	cataclastic texture	78.8	0.75	6.44	7.43	0.90	4.14	55.71	6.75
FK16-A9-2	1.6	23.16	semibright coal	cataclastic texture	86.7	0.73	6.62	7.73	1.01	4.76	61.53	5.24
FK18-A5-3	1.57	1.78	semibright coal	cataclastic texture	83.5	0.71	9.13	9.92	0.79	5.47	55.13	9.74
FK18-A5-4	1.42	9.71	semibright coal	cataclastic texture	95.6	0.66	10.63	11.50	0.87	5.66	49.19	9.64
FK18-A5-5	1.48	3.97	semibright coal	cataclastic texture	90.7	0.69	10.36	11.33	0.98	6.54	57.77	9.88
FK2-A3-1	2.66	8.12	semibright coal	cataclastic texture	94.9	0.51	5.50	6.20	0.70	4.03	64.96	6.86
FK2-A3-10	2.45	4.63	semibright coal	cataclastic texture	72.3	0.57	7.22	7.67	0.45	3.36	43.83	6.01
FK2-A3-2	2.44	9.55	semibright coal	cataclastic texture	95.6	0.52	5.91	6.48	0.57	3.50	54.07	6.06

https://doi.org/10.1021/acsomega.3c04911
ACS Omega 2023, 8, 40417−40432

Table 1. continued

coal sample	M_{ad} (%)	A_d (%)	coal rock type	coal mass structure	vitrinite content (%)	$R_{o,max}$ (%)	total desorption amount (cm^3/g)	gas content (cm^3/g)	lost gas content (cm^3/g)	total desorption volume in the first 8 h (cm^3/g)	desorption ratios (%)	on-site average desorption rate ($\times10^{-3}\cdot cm^3/g\cdot min^{-1}$)
FK2-A3-3	2.66	7.34	semibright coal	cataclastic texture	91.3	0.53	6.29	6.80	0.51	3.73	54.84	6.65
FK2-A3-4	2.35	6.02	semibright coal	cataclastic texture	71.2	0.53	6.22	6.69	0.46	2.92	43.70	5.08
FK2-A3-5	2.77	5.19	semibright coal	cataclastic texture	92.5	0.54	6.69	7.27	0.58	3.74	51.41	6.51
FK2-A3-6	2.62	5.6	semibright coal	cataclastic texture	71.5	0.54	6.09	6.69	0.60	4.00	59.82	7.01
FS-24-39B-1	1.64	7.11	semibright coal	cataclastic texture	91.5	0.69	12.03	13.28	1.24	7.57	56.97	13.18
FS-24-39B-3	1.58	6.88	semibright coal	cataclastic texture	85.1	0.66	8.05	9.18	1.13	6.46	70.42	11.11
FS-24-41-1	1.61	3.72	semibright coal	cataclastic texture	87.4	0.72	15.68	17.73	2.01	10.70	60.36	18.10
FS-24-42-12	1.26	3.82	semibright coal	cataclastic texture	94.3	0.75	11.92	13.40	1.49	8.84	65.99	15.33
FS-24-42-18	1.08	10.23	semibright coal	cataclastic texture	96.7	0.77	11.11	12.89	1.78	10.23	79.36	17.59
FS-24-44-13	1.37	5.62	semibright coal	cataclastic texture	70.6	0.94	7.33	7.91	0.58	3.57	45.08	6.22
FS-24-44-4	1.27	1.73	semibright coal	cataclastic texture	80.4	0.86	16.47	17.22	0.76	5.46	31.71	9.79
FS60-39[1]-1	1.77	21.41	semibright coal	cataclastic texture	95.8	0.68	6.58	7.40	0.82	4.36	58.90	7.30
FS60-39[2]-2	1.26	30.05	semibright coal	cataclastic texture	94.2	0.64	5.36	6.56	1.20	4.31	65.75	6.42
FS60-39[2]-3	1.65	27.2	semibright coal	cataclastic texture	95	0.66	6.54	7.05	0.51	3.46	49.15	6.09
FS60-41-1	1.56	36.25	semibright coal	cataclastic texture	82.9	0.71	7.54	8.82	0.30	2.16	24.45	3.82
FS60-41-2	1.56	36.25	semibright coal	cataclastic texture	88.9	0.71	7.23	8.20	0.97	5.46	66.56	9.25
FS60-41-3	1.55	13.85	semibright coal	cataclastic texture	83.3	0.77	8.08	8.54	0.45	3.41	39.96	6.10
FS60-41-4	1.36	11.18	semibright coal	cataclastic texture	94.7	0.76	9.33	10.40	1.07	5.91	56.86	9.99
FS60-41-6	1.55	11.31	semibright coal	cataclastic texture	94.7	0.72	9.20	10.16	0.94	5.63	55.41	9.68
FK6-45-2-4	2.32	1.78	semibright coal	primary structure	58	0.65	6.27	7.25	0.91	4.59	63.29	7.67
FS-58-42-4	1.54	17.13	semibright coal	primary structure	94.2	0.59	4.91	5.91	0.13	1.17	19.73	2.15
FS-58-42-11	1.68	8.23	semibright coal	primary structure	98	0.56	5.42	6.53	0.13	0.97	14.87	1.75
FS-58-42-19	1.83	3.13	semibright coal	primary structure	86.6	0.62	6.28	7.95	0.18	1.75	22.03	3.28

characteristics and their influence factors could guide the effective development of CBM.

Cumulative desorption volume, desorption ratio, desorption rate, and adsorption time are the dominant parameters to evaluate the desorption characteristics of CBM.[9] The cumulative desorption volume is the sum of the individual stage desorption volumes, and the desorption ratio is the ratio of the sum of the lost and two h desorption volumes in the field to the total gas content. As for the desorption rate, it is the amount of gas desorbed per unit time, which is characterized by the adsorption time; it can be featured when the desorption volume reaches 63.2% of the total desorption volume. In China, the CBM desorption volume varies between 3.50 and 26.11 cm^3/g,[10] and the CBM desorption ratio is approximately below 70%.[11] In China, the desorption rate mostly varies between 1.05 and 61.23 $\times 10^{-3}$ mL/(g·min).[12] In the Xinjiang area, the adsorption time of low-rank coal is 0.0263−3.0417 d, and the desorption rate decays rapidly. Compared with that in the Daning−Jixian area, the adsorption times of medium- and high-rank coal are mainly 0.0438−9.958 d and 0.1158−20.5667 d,[11] respectively; the desorption rate decays slowly. Clearly, the higher the coal rank, the slower the desorption rate decays and the longer the desorption time. The former studies showed that the reservoir temperature,[13,14] pressure,[15] and internal factors, such as coal metamorphism,[16] structure,[17] rock,[18] quality,[19,20] and pore structure,[21,22] are dominant factors that could influence the desorption characteristics.

The influence of different factors on desorption characteristics by setting different experimental parameters has been reported by former scholars. Yang et al.[23] screened coal samples with various particle sizes and conducted adsorption and desorption experiments at different temperatures; it was reported that the increased temperatures aggravate the thermal motion of gas molecules in pores, leading to increased gas

https://doi.org/10.1021/acsomega.3c04911
ACS Omega 2023, 8, 40417−40432

Table 2. High-Pressure Mercury Compression Test Pore Parameters

			stage pore volume (10^{-3}·cm^3/g)				percentage of pore volume (%)					
coal sample	total porosity (%)	total pore volume (cm^3/g)	micropore	transitional pore	mesopore	macropore	micropore	transitional pore	mesopore	macropore	open pore ratio (%)	proportion of semi-closed holes (%)
FC-2-39-3	4.5	0.06	14.19	24.80	6.57	14.44	23.66	41.33	10.95	24.07	23.46	76.54
FC-2-41-1	6.4	0.21	17.98	46.23	54.37	91.42	8.56	22.02	25.89	43.53	53.72	46.28
FS60-39^2-1	7.1	1.95	444.98	754.95	177.89	572.18	22.82	38.72	9.12	29.34	33.97	66.03
FS-24-39-1	2.8	0.13	31.51	53.84	11.00	33.66	24.24	41.41	8.46	25.89	28.53	71.47
FS-24-39-3	3.5	0.22	36.77	61.30	27.72	94.21	16.71	27.86	12.60	42.82	52.43	47.57
FS-24-39-5	8.5	0.17	16.30	35.24	15.88	102.58	9.59	20.73	9.34	60.34	69.56	30.44
FS-24-40-3	4.9	0.16	39.31	61.82	30.15	28.72	24.57	38.64	18.84	17.95	33.45	66.55
FS-24-41-8	6.2	0.18	20.45	70.84	20.21	68.49	11.36	39.36	11.23	38.05	42.19	57.81
FS-24-42-9	3.5	0.17	33.96	56.42	9.92	69.70	19.97	33.19	5.83	41.00	39.03	60.97
FS-24-43-1	3.9	0.14	16.56	41.94	20.62	60.88	11.83	29.96	14.73	43.48	54.62	45.38
FS-24-43-2	3.9	0.29	51.91	104.10	52.76	81.23	17.90	35.90	18.19	28.01	49.57	50.43
FS60-41-7	4.2	2.37	401.71	728.99	365.22	874.09	16.95	30.76	15.41	36.88	44.78	55.22
FS60-41-8	6.4	2.97	469.15	763.14	197.01	1540.70	15.80	25.69	6.63	51.88	54.42	45.58
FC-2-41-4	4.5	0.08	14.42	27.23	10.80	27.54	18.03	34.04	13.50	34.43	42.89	57.11
FC-2-41-5	2.1	0.07	10.86	23.14	8.79	27.21	15.51	33.06	12.56	38.87	54.76	45.24
FS60-41-5	5.3	2.35	341.23	641.59	409.48	957.70	14.52	27.30	17.42	40.75	52.32	47.68
FC-2-39-1	2.6	0.11	23.00	39.59	11.23	36.17	20.91	36.00	10.21	32.88	35.82	64.18
FC-2-39-2	2.6	0.04	11.16	18.32	3.36	7.17	27.89	45.79	8.41	17.91	18.80	81.20
FC-2-41-2	6.6	0.15	12.44	30.56	38.07	68.93	8.30	20.37	25.38	45.95	58.63	41.37
FC-2-41-3	1.7	0.05	10.63	21.56	5.78	12.04	21.25	43.12	11.55	24.08	42.06	57.94
FS60-39^1-1	8.5	6.22	459.25	929.44	529.06	4302.26	7.38	14.94	8.51	69.17	77.32	22.68
FS60-39^2-2	3.9	2.79	455.78	860.46	538.45	935.31	16.34	30.84	19.30	33.52	52.42	47.58
FS60-39^2-3	4.6	1.13	256.20	441.10	108.95	323.75	22.67	39.04	9.64	28.65	35.76	64.24
FS60-41-1	1.9	1.09	267.03	465.17	101.06	256.74	24.50	42.68	9.27	23.55	28.16	71.84
FS60-41-2	2.8	1.7	325.36	611.54	171.92	591.18	19.14	35.97	10.11	34.78	42.20	57.80
FS60-41-3	2.1	1.21	309.33	535.13	103.55	261.98	25.56	44.23	8.56	21.65	24.63	75.37
FS60-41-4	2.9	1.95	414.56	711.23	185.08	639.13	21.26	36.47	9.49	32.78	35.98	64.02
FS60-41-6	2.7	1.82	378.96	640.58	142.64	657.82	20.82	35.20	7.84	36.14	39.63	60.37
FS-24-39B-1	4.2	0.18	29.08	51.52	13.18	86.22	16.15	28.62	7.32	47.90	51.33	48.67
FS-24-39B-3	4.9	0.19	40.54	66.76	12.57	70.14	21.34	35.13	6.62	36.91	40.12	59.88
FS-24-41-1	8.3	0.31	52.27	92.62	36.90	128.20	16.86	29.88	11.90	41.35	55.70	44.30
FS-24-42-12	4	0.17	29.24	43.94	9.83	86.99	17.20	25.84	5.79	51.17	52.78	47.22
FS-24-42-18	4.8	0.18	26.01	65.51	21.37	67.11	14.45	36.39	11.87	37.29	41.09	58.91
FS-24-44-4	3.8	0.15	47.67	67.40	12.09	22.84	31.78	44.93	8.06	15.23	22.39	77.61
FS-24-44-13	6.3	0.41	34.05	108.33	119.17	148.46	8.30	26.42	29.06	36.21	56.61	43.39

diffusion and desorption rates, and it finally enhances the desorption capacity. Du et al.[24] ground and screened the coal particles to a size of 1−3 mm, and then the desorption characteristics under different pressure conditions were evaluated; it showed that the higher the adsorption equilibrium pressure of the coal gas, the higher the CBM cumulative desorption volume and desorption rate would be, which is beneficial to CBM desorption and diffusion. Yan et al.[5] selected experimental samples comprising particle sizes ranging from 0.25 to 0.18 mm and conducted isothermal adsorption experiments by constructing a single-pore diffusion model; the effective diffusion coefficient of methane first decreased and then increased with increasing coal rank. Zhaoping et al.[25] analyzed diffusion characteristics based on temporal desorption kinetic data in isothermal adsorption experiments for coals that had different body structures and found that the desorption and diffusion rates of tectonic coals were higher than those of primary coals. Ma et al.[26] studied the relationship between adsorption characteristics and macerals and found that the higher the vitrinite content, the higher the coal methane adsorption desorption capacity would be. Guo et al.[27] conducted desorption experiments on granular coal samples with a self-water injection device and found that moisture inhibited desorption. Zhao et al.[28] conducted adsorption and desorption experiments on coal samples that had particle sizes of 0.2−0.5, 0.5−1, and 1−3 mm at the same temperature and equilibrium pressure and found that the smaller coal particles commonly feature higher desorption volume. Peng et al.[29] prepared 4.2 mm diameter cylindrical coal cores to launch the permeability and desorption capacity measurements and found that a higher ash content would reduce the coal permeability and desorption capacity. Liu et al.[30] selected crushed coal samples (sieved through 60−80 mesh) to conduct adsorption−desorption experiments and found that during desorption the gas predominantly desorbed in large pores and that the desorption rate gradually decreased with decreasing pore size.

The desorption characteristics of coal in various areas of China with different maturities have been reported, although these were mostly derived from laboratory experiments conducted on artificially crushed coal samples that were treated with gas saturation first and then their desorption characteristics were investigated, which is different from natural desorption characteristics of raw coal core samples.

https://doi.org/10.1021/acsomega.3c04911
ACS Omega 2023, 8, 40417−40432

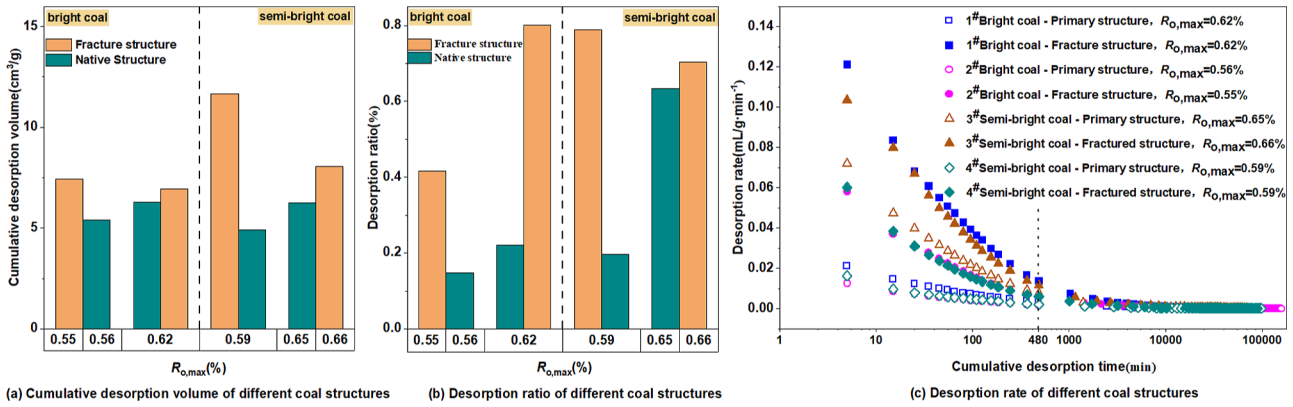

(a) Cumulative desorption volume of different coal structures (b) Desorption ratio of different coal structures (c) Desorption rate of different coal structures

Figure 1. Relationships between desorption characteristics and coal body structures.

Besides, studies on influence factors of desorption characteristics lack a systematic analysis of multiple factors, and the main controlling factors must be further clarified. Therefore, in this study, the high-pressure mercury injection, gas content, and natural desorption of 91 coal core samples collected from 11 CBM wells in the Fukang mine area in Xinjiang, China, were measured and are utilized to elucidate the desorption characteristics of coal samples that have different coal body structures and macrolithotypes. Furthermore, we investigated the effects of various coal quality parameters that were selected to investigate the influence on the coal desorption characteristics, including the maximum reflectance and content of the specular group, moisture content, ash yield content, and volumetric proportions of micropores, medium and large pores, and open-pore percentages. Finally, the main control factors that affect the desorption characteristics were discussed multiple times, which can provide a theoretical basis for managing coal mine gas disasters and efficiently developing CBM.

2. SAMPLES AND METHODS

In this study, 91 coal core samples were collected from 11 CBM wells in the Fukang mine area. The sample parameters, including the coal body structure, coal rock characteristics (macrolithotype, vitrinite content, and maximum reflectance of vitrinite), coal quality characteristics (moisture content and ash yield), pore characteristics (micro- and macroporosities, volumetric proportion of micro- and macropores, and open-pore percentage), and gas content and desorption characteristics, are collated in Table 1. These parameters were determined based on the following standards: the classification of coal body structures refers to "GB/T 30050-2013 Classification of Coal Body Structure," and the coal body structures could be divided into primary structure coal, cataclastic structure coal, granulated structure coal, and mylonitic structure coal. The classification of macrolithotype refers to "GB/T 18023-2000 Classification of Macroscopic Coal Rock Type of Bituminous Coal," and the macrolithotype includes bright, semibright, semidull, and dull coals. The classification of microscopic coal rock components refers to "GB/T 8899-2013 Determination Method of Microscopic Component Group and Mineral of Coal," vitrinite, inertinite, exinite, and minerals. The division of coal quality refers to the "GB/T 212-2008 Industrial Analysis Method of Coal", which is divided into moisture content (M_{ad}), ash yield (A_d), and volatile matter (V_{daf}). Vitrinite reflectivity refers to "GB/T 6948-2008 Vitrinite Reflectivity of Coal." The pore size distribution and porosity of solid materials were determined using mercury pressure and gas adsorption methods, respectively. Gas content determination refers to "GB/T 19559-2008 Coalbed Methane Content Determination Method", after 8 h of desorption in the field, the coal samples were sealed in a desorption tank and sent to the laboratory for desorption. Natural desorption continued for an average of seven consecutive days at not more than 10 cm^3 per day, and then the desorption was finished. The high-pressure mercury compression test refers to the "GB/T 21650.1-2008 Mercury intrusion method and Gas Adsorption Method for Determination of Pore Size Distribution and Porosity of Solid", and the results are shown in Table 2.

Cataclastic structure coal mainly developed in the study area, along with a small amount of primary coal. As for the macroscopic coal rock, bright and semibright coals were mainly developed in the study area. Therefore, this study focuses on the comparative analysis of the natural desorption characteristics of coal samples obtained from a coal body-macrolithotype comprising cataclastic structure-bright and semibright coals.

In this study, desorption parameters, including cumulative desorption volume, desorption ratio, and desorption rate, were selected to characterize the natural desorption characteristics of coal samples. Due to the natural desorption characteristics of the coal, the average on-site desorption rate, which can be described as the ratio of the cumulative desorption volume during 8 h of on-site desorption to the 8 h duration, was selected and was used to characterize the natural desorption characteristics; the desorption ratio was characterized based on the loss amount and cumulative desorption volume in the first 8 h to the total gas content.

3. RESULTS

3.1. Desorption Characteristics of Coal with Different Coal Structures. The in-field natural desorption experiments showed that the cumulative desorption volume, desorption ratio, and on-site average desorption rate of cataclastic structure coal were higher than those of primary structure coal under the same macrolithotype and same or similar vitrinite reflectivity conditions. (1) The cumulative desorption volume of cataclastic structure-bright and semibright coals were higher than those of primary structure-bright and semibright coals and were above 5 cm^3/g (Figure 1a). (2) The desorption ratios of both cataclastic structure-bright and

https://doi.org/10.1021/acsomega.3c04911
ACS Omega 2023, 8, 40417−40432

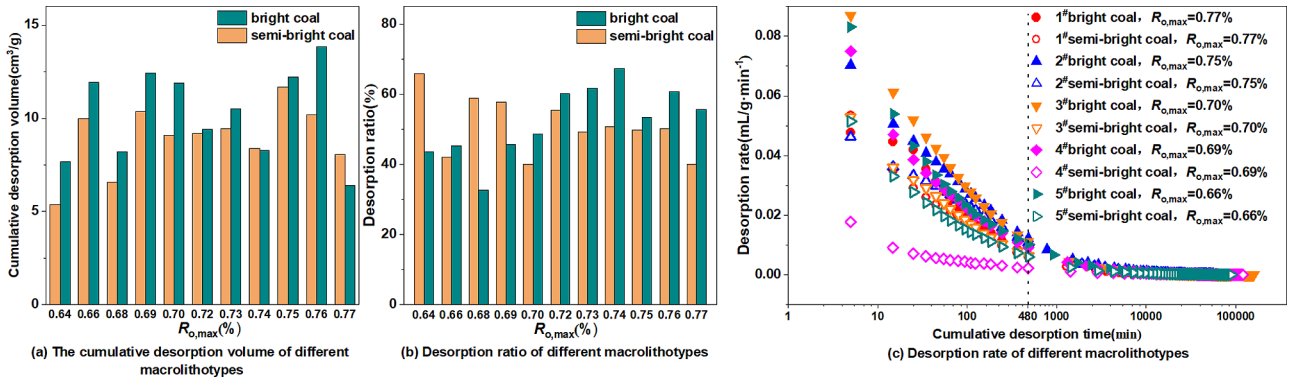

(a) The cumulative desorption volume of different macrolithotypes (b) Desorption ratio of different macrolithotypes (c) Desorption rate of different macrolithotypes

Figure 2. Desorption characteristics of different macrolithotypes.

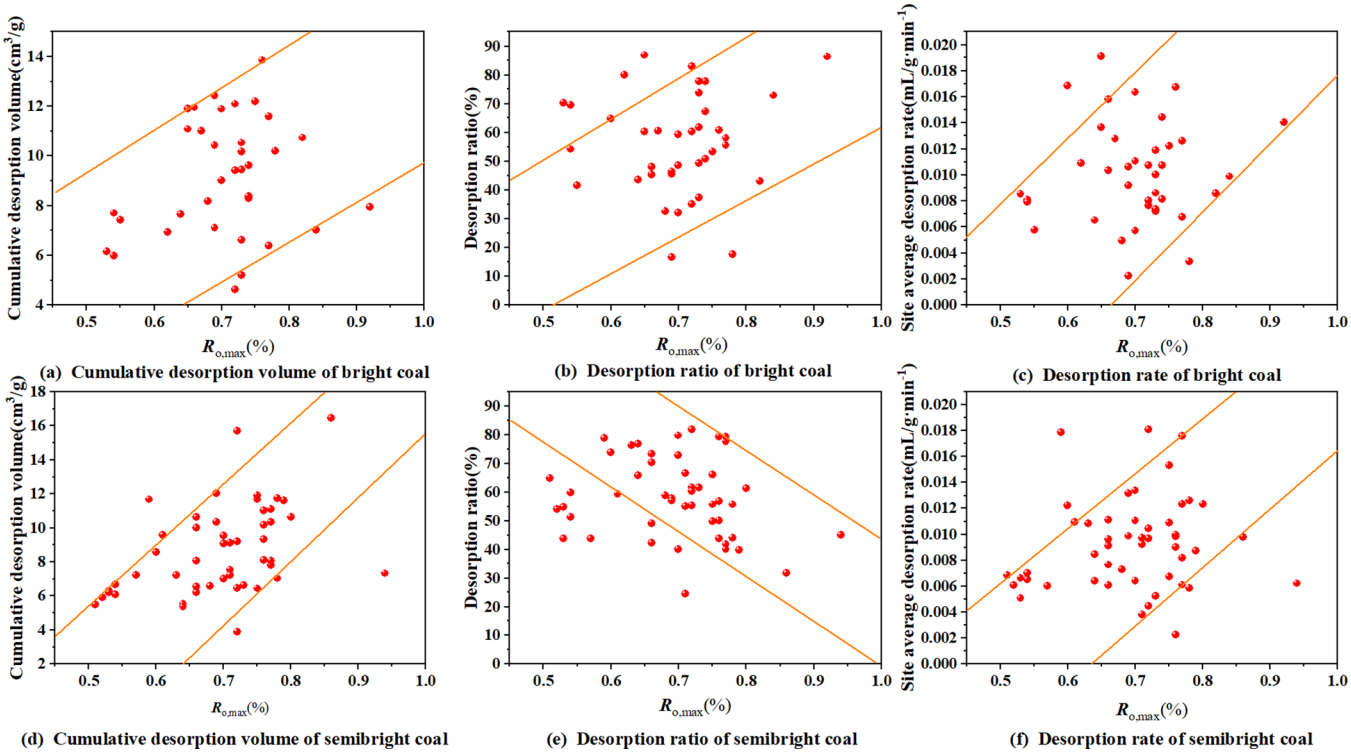

(a) Cumulative desorption volume of bright coal (b) Desorption ratio of bright coal (c) Desorption rate of bright coal

(d) Cumulative desorption volume of semibright coal (e) Desorption ratio of semibright coal (f) Desorption rate of semibright coal

Figure 3. Relationships between desorption characteristics and vitrinite reflectivity.

semibright coals were higher than those of primary structure-bright and semibright coals and were above 40% and up to 80%, respectively (Figure 1b), which were 2.9 times higher than those of the primary structure coals on average. (3) The initial desorption rates of cataclastic structure-bright and semibright coals were higher than those of primary structure-bright and semibright coals, and the desorption rate decayed faster for cataclastic structure coals than for primary structure coals. The desorption rates of both cataclastic structure and primary structure coals gradually decreased to below 0.02 mL/(g·min) after 480 min of in-field desorption. The on-site average desorption rate of cataclastic structure coals was 2.8 times higher than that of primary structure coals, and the desorption rates of both cataclastic structure and primary structure coals approached 0 after 10,000 min of desorption (Figure 1c).

3.2. Desorption Characteristics of Coal with Different Macrolithotypes. The cataclastic structure coal is mostly developed in the study area; the desorption characteristics of different macrolithotype in cataclastic structure coals were investigated. The data analysis showed that the cumulative desorption volume, desorption ratio, and desorption rate of cataclastic structure coals containing different macrolithotypes were bright > semibright coals under the same or similar sample reflectance conditions (Figure 2). The cumulative desorption volumes of both bright and semibright coals were above 5 cm^3/g, and the cumulative desorption volume of bright coals was higher than that of semibright coals by 72.73% (Figure 2a). The desorption ratios of all of the samples were below 80%, and the overall average desorption ratio was only approximately 40%. The desorption ratio percentage of bright coal was 72.73% higher than that of semibright coal (Figure 2b). Although the desorption rates of both bright and semibright coals showed the same trend and both gradually decreased with prolonged desorption, the initial desorption rate of bright coal was higher than that of semibright coal, and the on-site average desorption rate of bright coal was 1.5 times higher than that of semibright coal (Figure 2c).

https://doi.org/10.1021/acsomega.3c04911
ACS Omega 2023, 8, 40417−40432

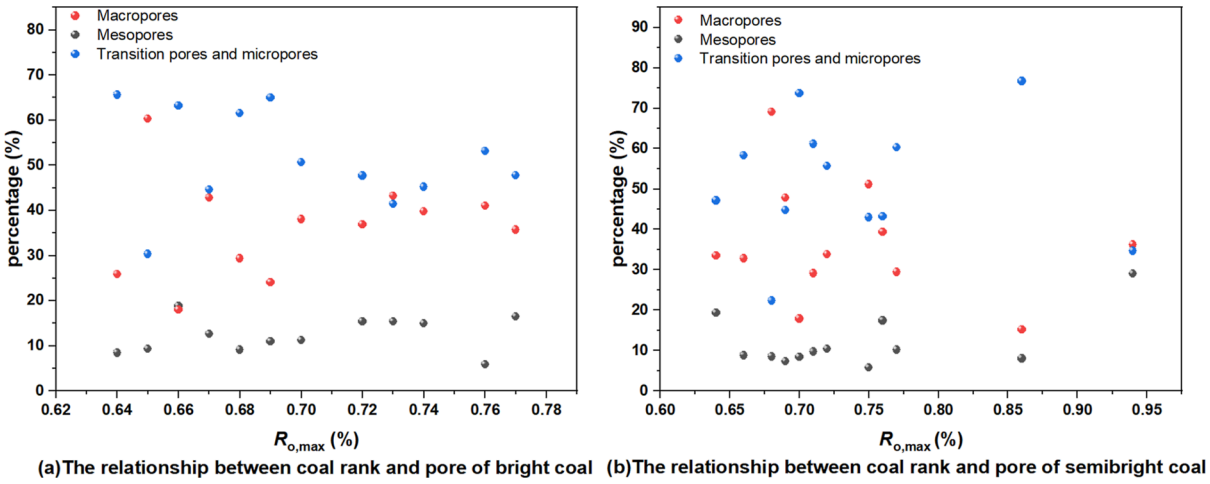

Figure 4. Relationships between vitrinite reflectivity and percentage of pore volume.

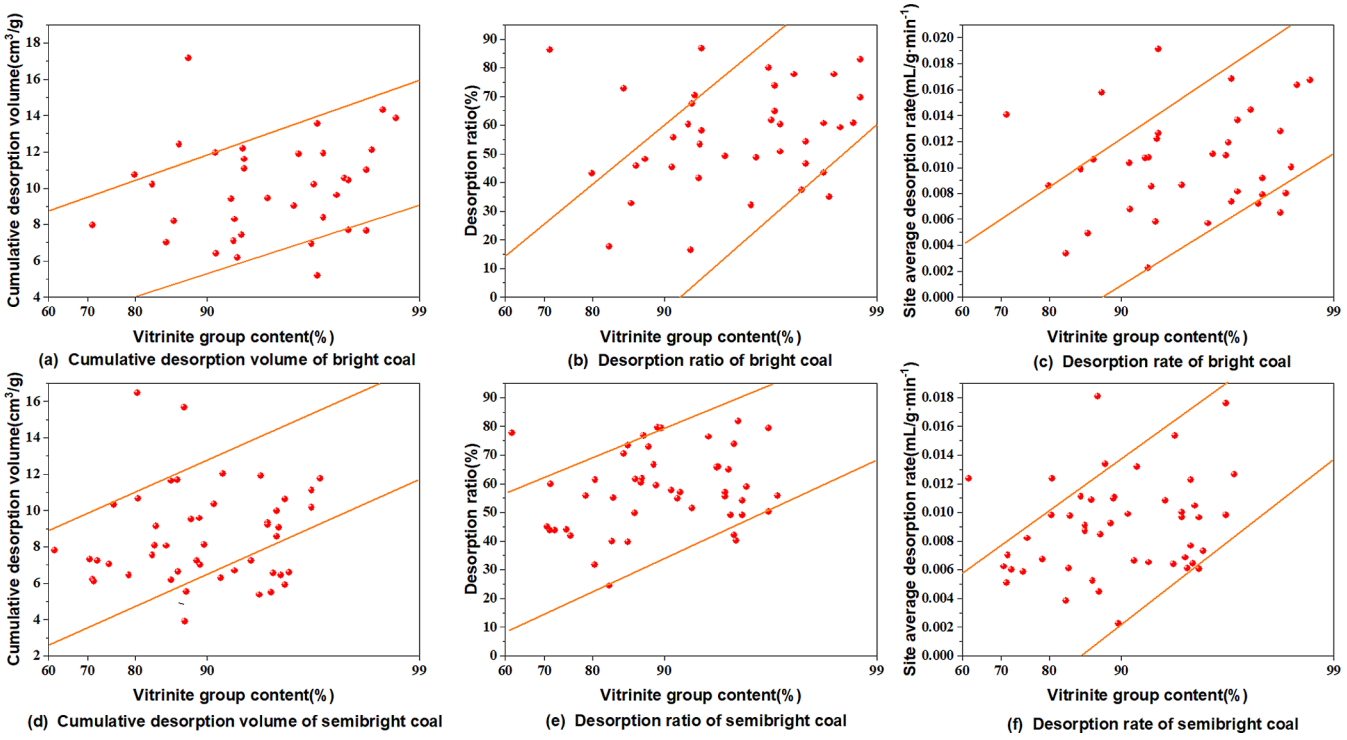

Figure 5. Relationships between desorption characteristics and content of vitrinite group.

4. ANALYSIS AND DISCUSSION

4.1. Coal Body Structure and Macrolithotype. Under the natural desorption condition, coal gas diffuses from the pore to the fracture and then migrates to the outer surface under a concentration gradient. For cataclastic coal, the number of gas migration channels increases and the gas diffusion path shortens.[31] Besides, it changes the proportion of pore types. Compared with primary coal, cataclastic coal contains large amounts of medium and large pores and fewer closed pores, and the pore connectivity and desorption capacity both increase.[17,32,33]

Macrolithotypes are divided according to the contents of bright components (vitrain and clarain coal); the bright component content of bright coal is more than 80%, and the bright component content of semibright coal is between 50 and 80%. The difference in desorption characteristics with different macrolithotypes is essentially caused by the difference in bright components.[34] On the one hand, vitrain coal is texturally pure, structurally uniform, and often lenticular or banded and has endogenous fissures that bear vertical bands.[35] The connectivity of the pore is good, and the gas desorption capacity is high. Clarain coal is not as uniform as vitrain coal, endogenous fissures are not as good as those in vitrain coal, and the desorption capacity is worse than that of vitrinite coal. On the other hand, the vitrinite content of vitrain is greater than that of clarain coal, and the vitrinite is hydrophobic,[36,37] which leads to a lower moisture content in vitrain and less influence on the gas diffusion resistance. Therefore, the desorption capacity of vitrain is higher than that of clarain coal. The difference in the contents of vitrain and clarain coal changes the desorption effect. Overall, the desorption capacity of bright coal is higher than that of semibright coal.

https://doi.org/10.1021/acsomega.3c04911
ACS Omega 2023, 8, 40417−40432

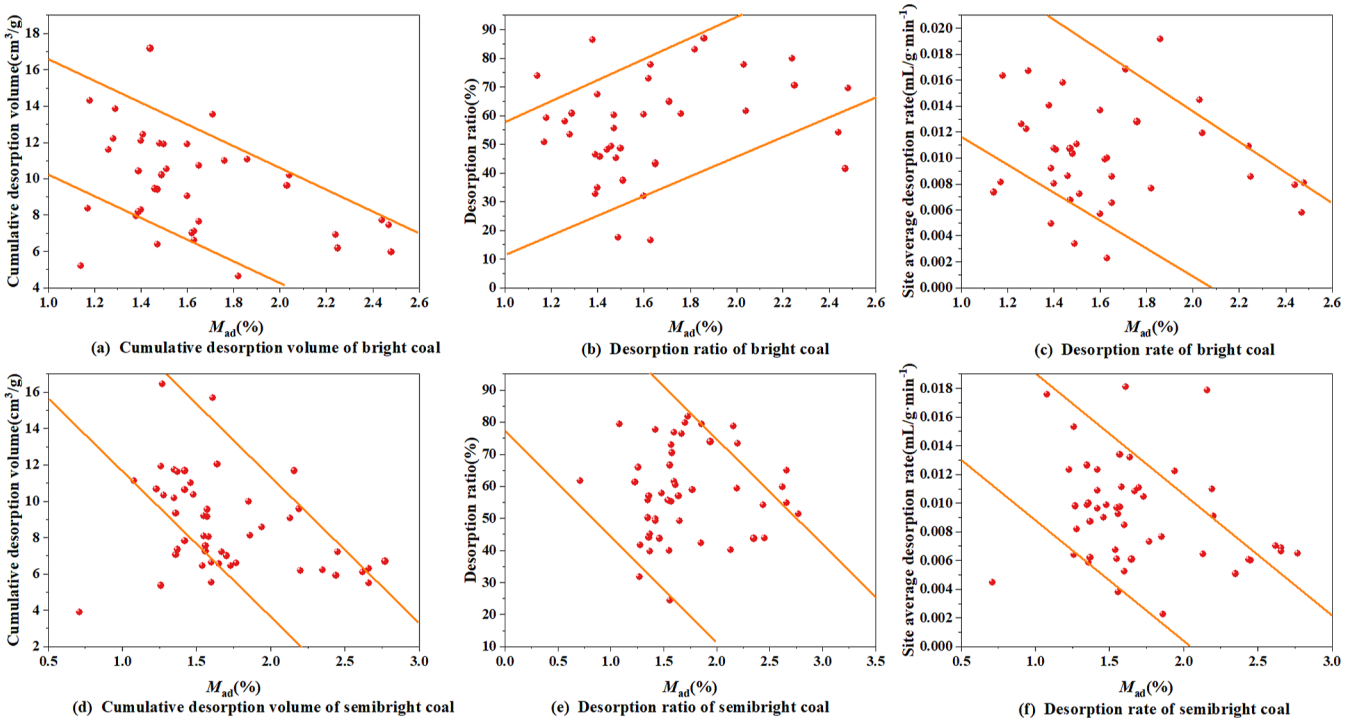

Figure 6. Relationships between desorption characteristics and moisture content.

4.2. Maximum Reflectance of Vitrinite. For cataclastic structure-bright coals, the cumulative desorption volume, desorption ratio, and on-site average desorption rate all increased overall with increasing maximum reflectance of vitrinite (Figure 3a−c). For cataclastic structure-semibright coals, although the cumulative desorption volume and on-site average desorption rate increased overall with increasing maximum reflectance of vitrinite (Figure 3d,f), the desorption ratio decreased instead (Figure 3e).

For the samples in the study area, the maximum vitrinite reflectance was relatively low (between 0.5 and 1%). For the coal with lower maturity, the spatial structure was loose, the aromatic lamellar spacing was large, and the side chain was long. With increasing coal rank, active functional groups continue to fall off, and the coal macromolecular structure substantially increases the condensation ring in the coal molecular structure, which decreases the number of side chains and functional groups and enables the growth degree of the coal microcrystalline structure to develop in an orderly direction. Therefore, the directional arrangement and anisotropy of coal molecules are both substantially improved, and the aromatic lamellae are arranged more closely. The coal structure stably evolves, which decreases porosity and meso- and macropore volumes.[38] When the vitrinite reflectance (*Ro*) is below 3%, the desorption ratio of CBM increases with increasing coal rank.[39]

The desorption ratios of bright and semibright coals (Figure 3) show different trends with increasing vitrinite reflectivity. From the pore characteristic analysis, in bright coals, the proportions of transition and micropores slightly decrease and the proportions of meso and macropores increase with increasing vitrinite reflectivity (Figure 4a), which improves the pore connectivity of bright coal and increases the initial desorption, and then the on-site desorption ratio increases. The increase in reflectance increases the proportions of micro- and transition pores and decreases the proportion of macropores in semibright coal (Figure 4b). The pore connectivity is poor and the initial desorption is low, so the desorption ratio decreases. Moreover, there were differing trends found in the pore characteristics of bright and semibright coal with varying vitrinite reflectivity. This is due to the higher content of vitrain and clarain coal in bright coal as compared to semibright coal. Vitrain coal typically shows fissures[35] which link closed pores and small pores. With an increase in vitrinite reflectivity, more tiny pores are developed, which leads to more fissure-connected pores. The proportion of tiny pores present in bright coal reduces with rising vitrinite reflectivity.

4.3. Coal Maceral Group. The vitrinite content of cataclastic structure-bright coal ranged from 70 to 98%, and the distribution was concentrated above 90% (Figure 5a−c). The vitrinite content of cataclastic structure-semibright coal ranged from 60 to 98%, and the distribution was more discrete (Figure 5d−f). The cumulative desorption volumes, desorption ratios, and on-site average desorption rates of cataclastic structure-bright and semibright coals were positively correlated with the vitrinite content.

The influence of the vitrinite content on the desorption characteristics of coal samples is mainly indicated by the following three aspects: (1) For functional groups, because the vitrinite group is rich in aliphatic and aromatic hydrocarbons, alkane side chains can more strongly adsorb methane. The more methane is adsorbed, the larger is the concentration difference that forms during desorption, which accelerates the initial desorption and increases cumulative desorption volume. (2) For moisture content, owing to very strong aliphatic C−H and more $-CH_2$ and $-CH_3$ stretching vibrations in vitrinite,[40] these side-chain functional groups have typical nonpolar surfaces and strong hydrophobicity.[41] In high-vitrinite-content coals, gas migration is less affected by moisture, and gas desorbs more easily. (3) For pore structures, in vitrinite, micropores are more developed, which provides a higher pore-

https://doi.org/10.1021/acsomega.3c04911
ACS Omega 2023, 8, 40417−40432

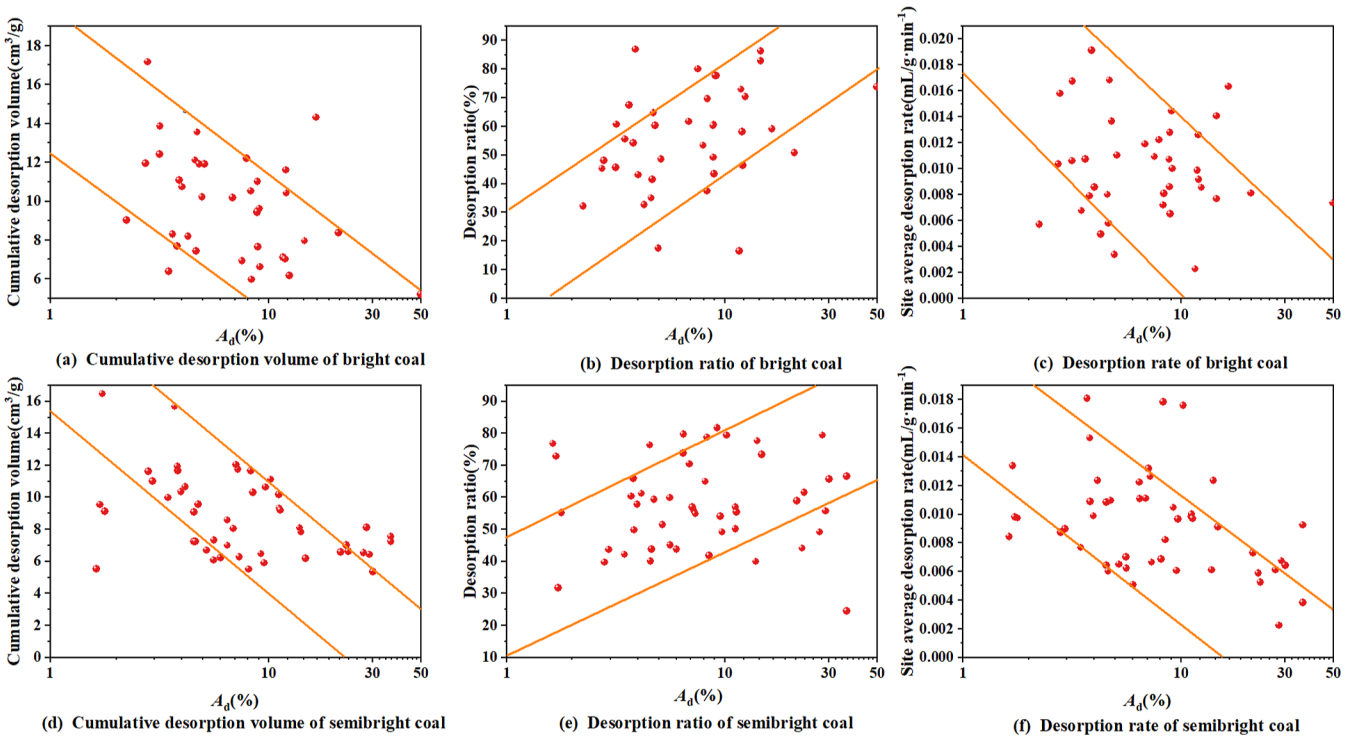

Figure 7. Relationships between desorption characteristics and ash yield.

specific surface area for CBM adsorption,[42,43] which increases the adsorption capacity. The larger the pressure difference that forms during desorption, the more gas that is emitted at the initial desorption stage, which accelerates desorption and increases cumulative desorption volume.

4.4. Coal Quality Characteristics. The moisture content of cataclastic structure-bright coals ranged from 1.1 to 2.6%, and these were distributed more discretely (Figure 6a–c). The moisture content of cataclastic structure-semibright coal ranged from 0.6 to 2.8% (Figure 6d–f), and the moisture content distribution was more concentrated at 1.5%. With the increased moisture content, the cumulative desorption volume and on-site average desorption rates of cataclastic structure-bright and semibright coals gradually decreased, and the desorption ratio gradually increased.

At different desorption stages, the influence of moisture on desorption characteristics is different. (1) In the original coal seam, the polarity of water molecules and affinity of coal-surface active sites, the coal matrix would be expanded and deformed after adsorbing water molecules,[44] which shortens and reduces the permeability of the effective methane seepage channel and finally reduces the methane desorption capacity. (2) During methane desorption, pressure gradient would be formed between the reservoir and the exterior, which promotes the outward migration of free methane in pores. During the initial migration procedure, the free methane must overcome the resistance of water molecules at pore walls and throats, which decreases the methane desorption capacity.[45] (3) As the reservoir pressure further decreases, adsorbed methane gradually desorbs because coal can adsorb water molecules more strongly than methane molecules. The adsorption potential of water-vapor molecules is approximately −24 kJ/mol, which is much higher than the methane adsorption enthalpy of approximately −2.704 kJ/mol.[46] During methane migration, free water molecules could replace the adsorbed CBM,[47] and water molecules absorb on the coal surface and form a water molecular film, which generates a certain vapor pressure and hinders the movement of gaseous molecules[48] and further obstructs methane migration. (4) As the reservoir pressure further decreases, free highly active methane molecules overcome the resistance, and it would gradually migrate out of the pore throat through the microfracture to the large pore and finally through the fracture-seepage output. When the gradient formed between the reservoir fluid and external pressures is below the throat resistance, gas molecules do not migrate in pores, which generates desorption hysteresis.

The methane desorption rates of bright and semibright coals in Figure 6 show the opposite trend because the methane desorption capacity of bright coal, as mentioned in Section 4.1, is higher than that of semibright coal, and coalbed fissures are more developed. Compared with the initial desorption capacity of semibright coal, that for bright coal is less affected by the increased water content. Because water molecules can adsorb on the coal surface more strongly than methane molecules, water molecules occupy methane adsorption points.[49] Therefore, the higher the water content, the lower the total gas content and higher the methane desorption rate of bright coal. For semibright coal, the methane desorption capacity is poor and substantially affected by the water content. The initial methane desorption and overall methane desorption rates both decrease with increasing water content.

The samples in the study area featured low-ash yield content, with ash yields ranging from 2 to 30 and 1 to 33% for bright and semibright coals, respectively (Figure 7). With the increased ash yields, the cumulative methane desorption volume and on-site average desorption rates of cataclastic structure-bright and semibright coals gradually decreased, and the desorption ratio gradually increased.

High-ash yield coal features significantly lower methane adsorption capacity than low-ash yield coal,[50] and the higher

https://doi.org/10.1021/acsomega.3c04911
ACS Omega 2023, 8, 40417−40432

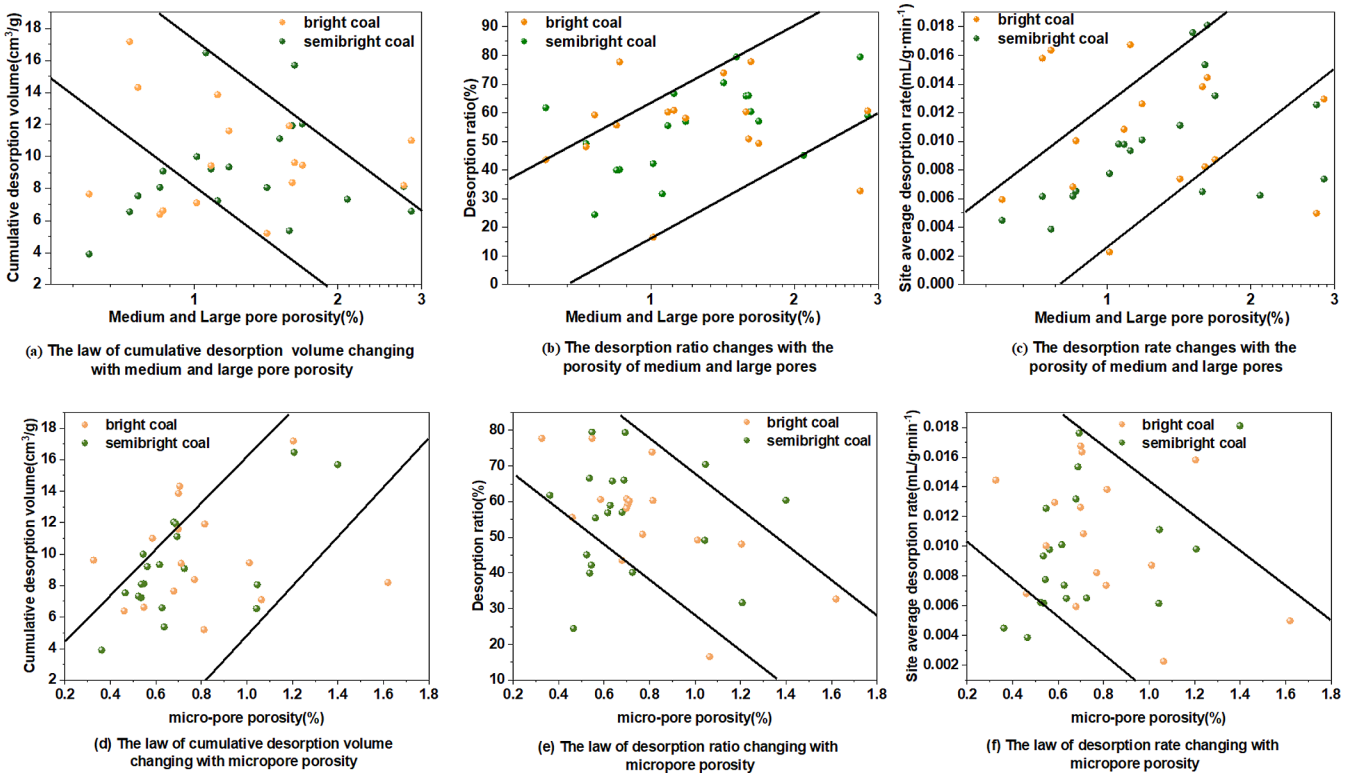

Figure 8. Relationships between desorption characteristics and porosity.

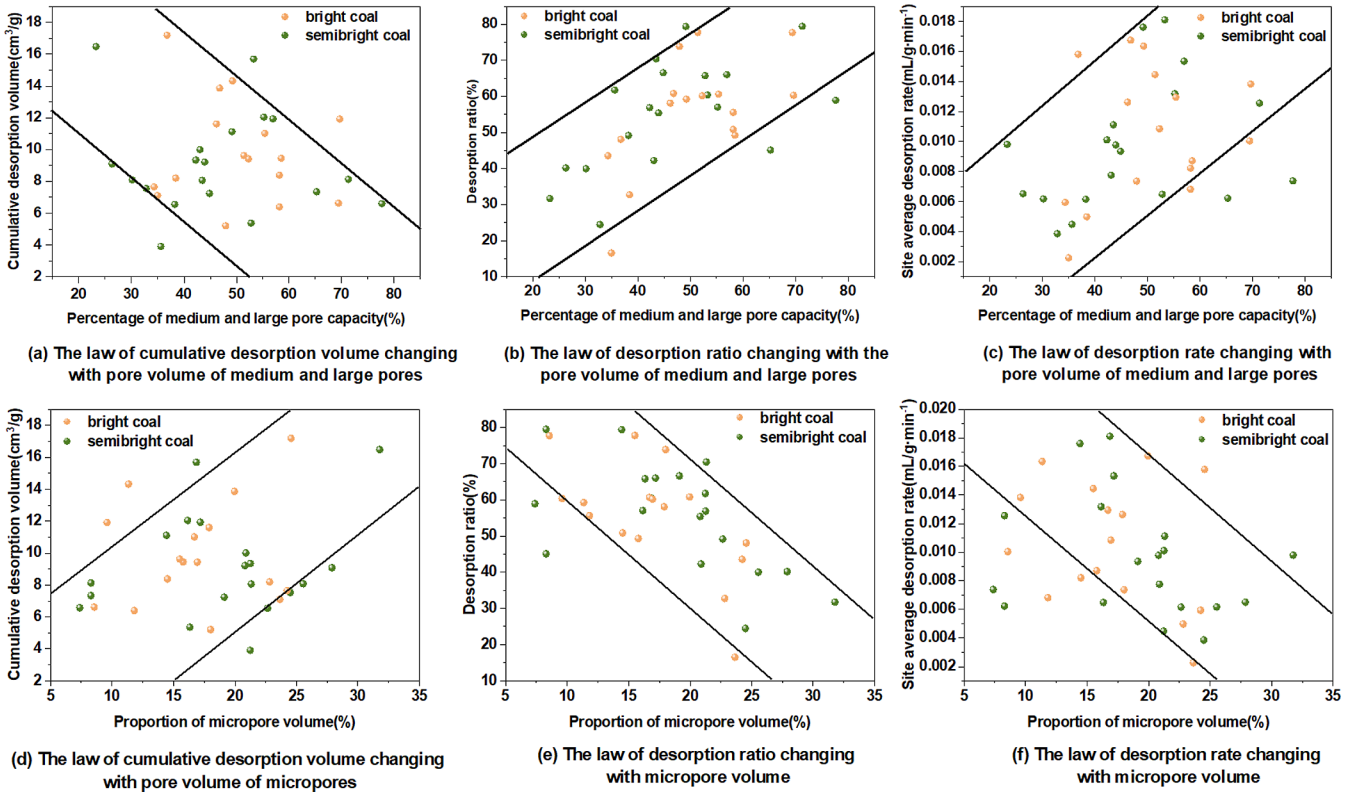

Figure 9. Relationships between desorption characteristics and the pore volume ratio.

the ash yield content, the lower the methane adsorption and cumulative desorption volume. On one hand, ash mostly comprises an inorganic mineral, which does not have any methane adsorption capacity. However, water molecules can chemically interact with inorganic substances on the coal surface and form hydrogen and chemical bonds, which enhance the interaction force between water molecules and the coal surface. This enhances the coal hydrophilicity, which

https://doi.org/10.1021/acsomega.3c04911
ACS Omega 2023, 8, 40417−40432

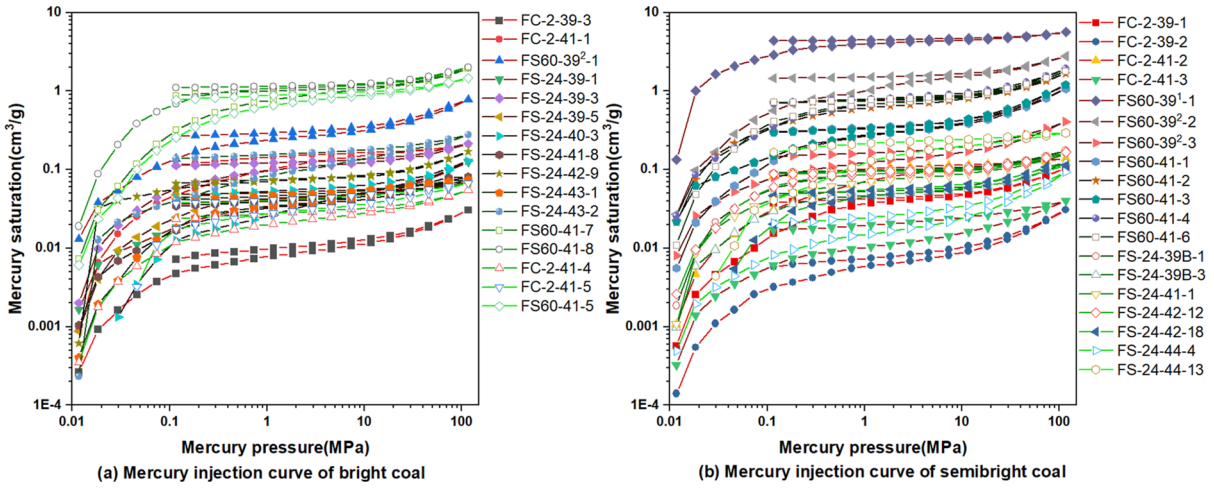

Figure 10. Mercury pressure curves of bright and semibright coals.

affects the amount of methane adsorbed and increases the desorption resistance. On the other hand, inorganic substances, such as clay minerals, can fill into pores and fractures in the coal,[51] which would occupy gas transport channels and substantially hinder gas diffusion and transport ability.

4.5. Pore Characteristics. *4.5.1. Porosity.* In this study, pores were classified into four various types according to the decimal pore size classification scheme, micropores (<10 nm), transition pores (from 10 to <100 nm), mesopores (from 100 to <1000 nm), and macropores (>1000 nm).[52] The micropores and transition pores are adsorption pores, and mesopores and macropores are seepage pores.[53,54] Overall, the coal samples exhibited a low metamorphic degree, and the mesopores and macropores were much more developed. The micropores have a large pore volume and pore-specific surface area,[55] and these types of pores are the main storage space for CBM adsorption. As diffusion and seepage channels for CBM, mesopores and macropores determine the strength of the initial desorption capacity.[56,57] Therefore, compared with the total porosity, the porosities of micro- and mesoporosities could more intuitively determine the methane desorption capacity.

In the cataclastic structure-bright and semibright coals collected in the study area, medium and large pore porosities varied from 0.2 to 3%, and the average cumulative methane desorption volume was approximately 10 cm^3/g. Additionally, the average methane desorption ratio was approximately 60%, and the on-site average desorption rate was approximately 0.01 $mL/(cm^3 \cdot g)$, which decreased while the desorption ratio and on-site average desorption rate both increased with increasing porosity (Figure 8a–c). Moreover, the microporosity was between 0.2 and 1.7%, and the cumulative methane desorption volume increased, while the desorption ratio and on-site average desorption rate both gradually decreased with increasing microporosity (Figure 8d–f).

On one hand, the amount of medium and large pores could increase the effective pore space in the coal seam, which can improve pore connectivity and then accelerate the diffusion of CBM. However, the micropores can increase both the adsorption space and cumulative desorption volume of CBM. Owing to the complexity of gas diffusion and seepage channels in micropores, gas migration is difficult, which slows and prolongs desorption and decreases the desorption ratio. On the other hand, the medium and large pores can reduce the amount of space occupied by pore water in the coal seam, which reduces the resistance of water to escape CBM. Therefore, the CBM desorption rate increases accordingly, and water fills micropores, which increases the micropore capillary resistance,[19] and desorption is not prominent.

4.5.2. Pore Volume Ratio. For the coal samples collected in the study area, the pore volume of medium and large pores ranged from 15 to 43%, and the cumulative desorption volume gradually decreased, while that for the desorption ratio and on-site average desorption rate featured opposition (Figure 9a–c). The proportion of the micropore volume was between 5 and 33%, and the cumulative methane desorption volume increased, while the desorption ratio and on-site average desorption rate both gradually decreased with the increasing proportion of micropore volume (Figure 9d–f). Compared with micropores and transition pores, medium and large pores usually have higher pore connectivity, which can provide larger pore space and faster gas diffusion, which play a key role in the initial desorption of coalbed methane.[30,58] Therefore, the higher the proportion of medium and large pore volumes, the stronger the desorption capacity, desorption ratio, and average desorption rate on site. Gas migrates in micropores mainly via Knudsen and transition diffusions.[59] During desorption, the gas migration path from the micropores lengthens, and the desorption time and rate slows down. Thus, the initial desorption capacity becomes weaker when the micropore volume proportion increases.

4.5.3. Percentage of Open Pores. The pores in the coal include effective and ineffective pores, and effective pores include open and semiclosed pores.[60] In mercury pressure experiments, the mercury withdrawal curve for open pores revealed a hysteresis loop due to the gradient between the inlet and withdrawal pressures, while that for semiclosed pores did not show a hysteresis loop because the inlet and withdrawal pressures were equal (Figure 10). The open-pore volume is the difference between the accumulated inlet and withdrawal mercury pressures while the semiclosed-pore volume is the accumulated withdrawal mercury presure,[9] and the open-pore percentage is the percentage of open pore volume to total pore volume.

The percentage of open-pores was mainly concentrated between 15 and 80%, and the cumulative desorption volume gradually decreased for both semibright and bright coals (Figure 11a), while the desorption ratio and on-site average

https://doi.org/10.1021/acsomega.3c04911
ACS Omega 2023, 8, 40417−40432

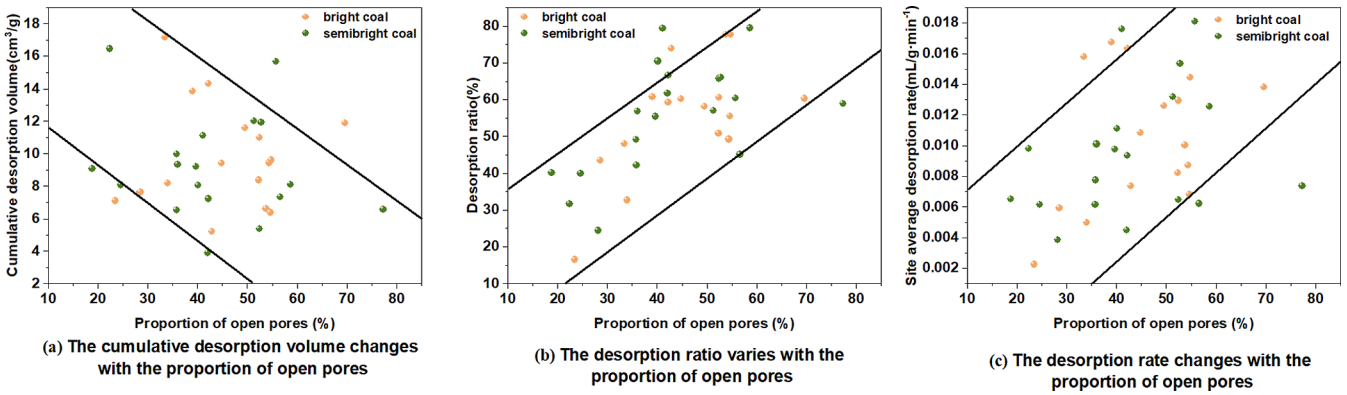

Figure 11. Relationships between desorption characteristics and open-pore percentage.

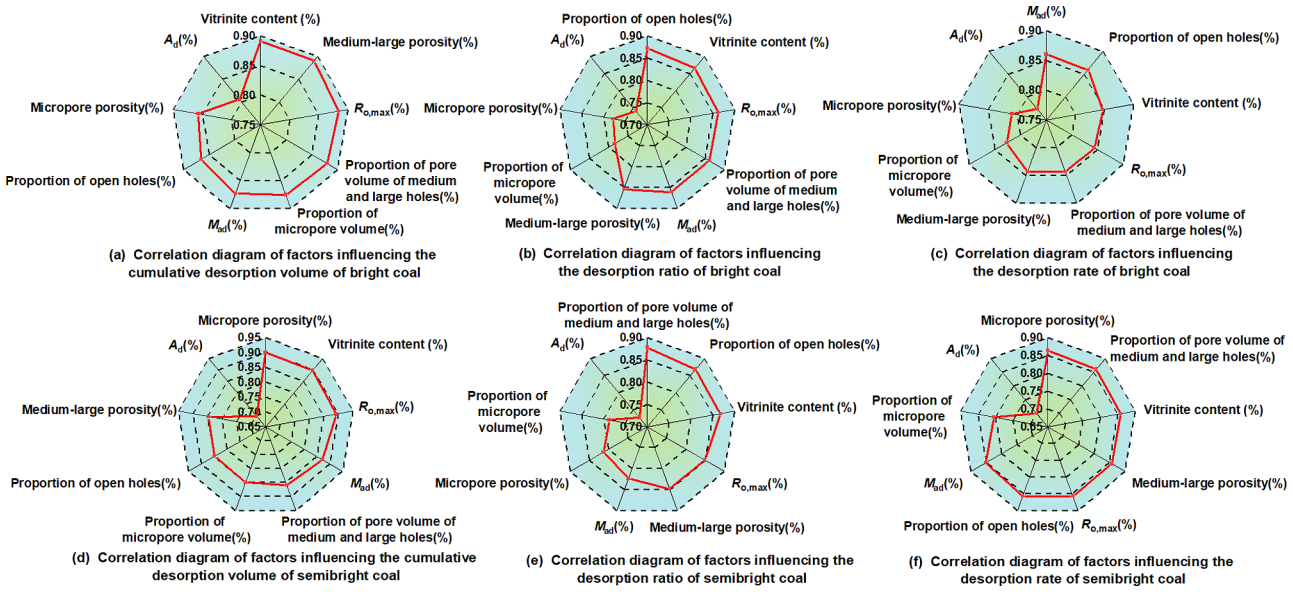

Figure 12. Principal factor analysis of desorption characteristics.

desorption rate of both semibright and bright coals gradually increased (Figure 11b,c) with increasing open-pore percentage.

The open pores mainly include cytosolic (plant tissue), intergranular, and mineral pores and fissures, and pores are connected to the coal outer surface, which enable gases or fluids to enter and exit freely.[38] This indicates that open pores feature a larger aperture. Desorption is a contrary procedure to adsorption; cumulative desorption volume should theoretically be positively correlated with methane adsorption in the coal body.[61] Additionally, in the coal body, methane adsorption mainly depends on microporosity.[55] Therefore, with an increasing number of open pores, methane adsorption and accumulated desorption both decrease. In addition, open pores favor the pore connectivity, which plays a decisive role in gas diffusion; that is, in coal, more open pores increase the number of diffusion channels in pore fissures, which improves the pore connectivity, increases both the desorption ratio and rate, and improves the desorption capacity.

4.6. Main Factor Analysis. Gray correlation analysis is a measure of the degree of correlation between factors by analyzing the degree of similarity or dissimilarity in their trends.[62] To study the relative magnitude of each factor for the degree of influence on desorption characteristics, the cataclastic structure-bright and semibright coals were selected as research objects, and SPSS software was used to analyze correlations among the maximum reflectance of the specular mass group, specular mass group content, moisture content, ash yield, pore characteristics (micro- and mesopore porosities, micro- and mesopore volumetric ratios, and open-pore ratio), and desorption characteristics. The correlations reveal the main controlling factors that affect the desorption characteristics.

The digital axis was selected as the start, and the correlation degree is arranged in a clockwise direction from high to low. The highest correlation degrees with the cumulative methane desorption volume, desorption ratio, and on-site average desorption rate of cataclastic bright coal are the content of vitrinite, medium and large pore contents, open-pore ratio, and water and vitrinite contents (Figure 12a–c). The highest correlation degrees with the cumulative desorption volume, desorption ratio, and on-site average desorption rate of the cataclastic structure-semibright coal are the vitrinite content, open-pore percentage, and vitrinite content (Figure 12d–f). The coal ash yield had the least influence on the desorption characteristics. The correlation degree of the first few factors is similar to that of the main factors owing to the comprehensive influence of multiple correlated factors on CBM desorption. For example, vitrinite is weakly hydrophilic, the moisture

https://doi.org/10.1021/acsomega.3c04911
ACS Omega 2023, 8, 40417−40432

content is affected, and the change in vitrinite reflectivity mainly affects the proportion of each pore diameter. Clearly, when influencing factors at different scales intersect, the correlation degree is similar after the main factor analysis.

5. CONCLUSIONS

(1) The cumulative natural desorption volume was between 5 and 15 cm^3/g for the Fukang mining area coal, and the average desorption ratio was 40%. The initial and on-site average desorption rates were below 0.14 and approximately 0.01 mL/ (g·min), respectively. The desorption capacities of cataclastic structure and bright coals were higher than those of primary and semibright coals, respectively.

(2) The percentage of adsorption pores in bright coal decreases as $R_{O,max}$ increases, and this results in a higher percentage of medium and large pores, which can improve the pore connectivity and increase the desorption ratio, whereas the semibright coal features the opposite. The vitrinite group exhibits developed micropores, resulting in a stronger methane adsorption capacity and larger concentration differences during desorption; consequently, coal samples with higher vitrinite content demonstrate stronger desorption capacity. An increased moisture and ash yield ultimately hinders gas diffusion and occupies adsorption points, reducing the cumulative desorption volume and average desorption rate at the site. The increase in microporous porosity and percentage of pore volume enhances gas adsorption capacity, resulting in a rise in cumulative desorption volume. The augmentation of medium and large pore porosity and volume enhances pore connectivity, and an increase in open pore augments gas seepage channels. Both these factors enhance the desorption rate and the on-site average desorption rate.

(3) The most significant effects on the cumulative desorption volume, desorption ratio, and on-site average desorption rate of bright coal are the vitrinite content and porosity of medium and large pores, open-pore percentage, M_{ad}, and vitrinite contents, respectively. For semibright coal, the crucial factors are microporosity, volumetric proportion of medium and large pores, and microporosity, respectively.

AUTHOR INFORMATION

Corresponding Authors

Haichao Wang − *Xinjiang Key Laboratory for Geodynamic Processes and Metallogenic Prognosis of Central Asian Orogenic Belt, Xinjiang University, Urumqi 830047, China; School of Geological and Mining Engineering, Xinjiang University, Urumqi 830047, China;* orcid.org/0000-0001-7830-6139; Email: wangxiaoshi2111@163.com

Zhenzhi Wang − *School of Resources & Environment, Henan Polytechnic University, Jiaozuo 454000, China;* orcid.org/0000-0002-1897-1310; Email: zhenzhiw6@163.com

Authors

Liang Du − *Xinjiang Key Laboratory for Geodynamic Processes and Metallogenic Prognosis of Central Asian Orogenic Belt, Xinjiang University, Urumqi 830047, China; School of Geological and Mining Engineering, Xinjiang University, Urumqi 830047, China*

Xuchao Huang − *China Coal Technology and Engineering Group Chongqing Research Institute, Chongqing 400037, China*

Zhengshuai Wang − *China Coal Technology and Engineering Group Chongqing Research Institute, Chongqing 400037, China*

Chuanjian Cheng − *China Coal Technology and Engineering Group Chongqing Research Institute, Chongqing 400037, China*

Kuwanixibieke Maimaitizhuma − *Xinjiang Key Laboratory for Geodynamic Processes and Metallogenic Prognosis of Central Asian Orogenic Belt, Xinjiang University, Urumqi 830047, China; School of Geological and Mining Engineering, Xinjiang University, Urumqi 830047, China*

Zhiwei Zeng − *Xinjiang Key Laboratory for Geodynamic Processes and Metallogenic Prognosis of Central Asian Orogenic Belt, Xinjiang University, Urumqi 830047, China; School of Geological and Mining Engineering, Xinjiang University, Urumqi 830047, China*

Bing Luo − *Xinjiang Key Laboratory for Geodynamic Processes and Metallogenic Prognosis of Central Asian Orogenic Belt, Xinjiang University, Urumqi 830047, China; School of Geological and Mining Engineering, Xinjiang University, Urumqi 830047, China*

Mengmeng Yang − *Xinjiang Key Laboratory for Geodynamic Processes and Metallogenic Prognosis of Central Asian Orogenic Belt, Xinjiang University, Urumqi 830047, China; School of Geological and Mining Engineering, Xinjiang University, Urumqi 830047, China*

Zheyuan Ouyang − *Xinjiang Key Laboratory for Geodynamic Processes and Metallogenic Prognosis of Central Asian Orogenic Belt, Xinjiang University, Urumqi 830047, China; School of Geological and Mining Engineering, Xinjiang University, Urumqi 830047, China*

Wei Dou − *Xinjiang Key Laboratory for Geodynamic Processes and Metallogenic Prognosis of Central Asian Orogenic Belt, Xinjiang University, Urumqi 830047, China; School of Geological and Mining Engineering, Xinjiang University, Urumqi 830047, China*

Beixi Zhang − *Xinjiang Key Laboratory for Geodynamic Processes and Metallogenic Prognosis of Central Asian Orogenic Belt, Xinjiang University, Urumqi 830047, China; School of Geological and Mining Engineering, Xinjiang University, Urumqi 830047, China*

Teng Li − *College of Petroleum Engineering, Xi'an Shiyou University, Xi'an 710065, China*

Complete contact information is available at: https://pubs.acs.org/10.1021/acsomega.3c04911

Notes

The authors declare no competing financial interest.

ACKNOWLEDGMENTS

This work was supported financially by the Xinjiang Uygur Autonomous Region Natural Science Foundation (2022D01C38), the National Natural Science Foundation of China Regional Fund (42262021), the National Natural Science Foundation of China Youth Fund (41902171), and the National Natural Science Foundation-Joint Fund Project (U1903303).

https://doi.org/10.1021/acsomega.3c04911
ACS Omega 2023, 8, 40417−40432

REFERENCES

(1) Dong, J.; Cheng, Y.; Jin, K.; Zhang, H.; Liu, Q.; Jiang, J.; Hu, B. Effects of diffusion and suction negative pressure on coalbed methane extraction and a new measure to increase the methane utilization rate. *Fuel* **2017**, *197*, 70−81.

(2) Wen, S.; Zhou, K.; Lu, Q. A discussion on CBM development strategies in China: A case study of PetroChina Coalbed Methane Co., Ltd. *Natural Gas Industry B* **2019**, *6* (6), 610−618.

(3) Palmer, I. Coalbed methane completions: A world view. *Int. J. Coal Geol.* **2010**, *82* (3−4), 184−195.

(4) Meng, Y.; Li, Z. Experimental study on diffusion property of methane gas in coal and its influencing factors. *Fuel* **2016**, *185*, 219−228.

(5) Yan, J.; Meng, Z.; Li, G. Diffusion characteristics of methane in various rank coals and the control mechanism. *Fuel* **2021**, *283*, 118959.

(6) Li, Z.; Liu, D.; Cai, Y.; Shi, Y. Investigation of methane diffusion in low-rank coals by a multiporous diffusion model. *J. Nat. Gas Sci. Eng.* **2016**, *33*, 97−107.

(7) Wang, K.; Wang, Y.; Xu, C.; Guo, H.; Xu, Z.; Liu, Y.; Dong, H.; Ju, Y. Modeling of multi-field gas desorption-diffusion in coal: A new insight into the bidisperse model. *Energy* **2023**, *267*, 126534.

(8) Shi, G.; Tao, M.; Zhang, H.; Yan, J.; Wen, Z. Study on gas desorption-diffusion behavior from coal particles using triple-pore structure models: Experimental, mathematical models, and numerical solutions. *Fuel* **2023**, *342*, 127731.

(9) Fu, X.; Qin, Y.; Wei, C. *Coalbed Methane Geology*; Xuzhou:China University of Mining and Technology Press, 2007; pp 81−87.

(10) Li, X.; Xie, G. Characteristics and effecting factors of adsorption time of coalbed gas reservoir. *Nat. Gas Geosci.* **2003**, *14* (06), 502−505.

(11) Li, J.; Liu, F.; Wang, H.; Zhou, W.; Liu, H.; Zhao, Q.; Li, G.; Wang, B. Desorption characteristics of coalbed methane reservoirs and affecting factors. *Petrol. Explor. Dev.* **2008**, *35* (1), 52−58.

(12) Zhang, H.; Yuan, Z.; Tian, X.; Wan, Z.; Pang, X.; Ma, S. Natural desorption rate and attenuation coefficient of coal seam gas and its significance. *Chinese Coalbed Methane* **2009**, *6* (04), 24−27.

(13) Charrière, D.; Pokryszka, Z.; Behra, P. Effect of pressure and temperature on diffusion of CO2 and CH4 into coal from the Lorraine basin (France). *Int. J. Coal Geol.* **2010**, *81* (4), 373−380.

(14) Li, X.; Wang, C.; Chen, Y.; Li, H. Influence of temperature on gas desorption characterization in the whole process from coals and its application analysis on outburst risk prediction. *Fuel* **2022**, *321*, 124021.

(15) Wang, K.; Ren, H.; Wang, Z.; Wei, J. Temperature-pressure coupling effect on gas desorption characteristics in coal during low-variable temperature process. *J. Pet. Sci. Eng.* **2022**, *211*, 110104.

(16) Laxminarayana, C.; Crosdale, P. J. Role of coal type and rank on methane sorption characteristics of Bowen Basin, Australia coals. *Int. J. Coal Geol.* **1999**, *40* (4), 309−325.

(17) Guo, H.; Yu, Y.; Wang, K.; Yang, Z.; Wang, L.; Xu, C. Kinetic characteristics of desorption and diffusion in raw coal and tectonic coal and their influence on coal and gas outburst. *Fuel* **2023**, *343*, 127883.

(18) Crosdale, P. J.; Beamish, B.; Valix, M. Coalbed methane sorption related to coal composition. *Int. J. Coal Geol.* **1998**, *35* (1−4), 147−158.

(19) Chen, M.; Chen, X.; Zhang, X.; Tian, F.; Sun, W.; Yang, Y.; Zhang, T. Experimental Study of the Pore Structure and Gas Desorption Characteristics of a Low-Rank Coal: Impact of Moisture. *ACS Omega* **2022**, *7* (42), 37293−37303.

(20) Chen, X.; Cheng, Y. Influence of the injected water on gas outburst disasters in coal mine. *Nat. Hazards* **2015**, *76* (2), 1093−1109.

(21) Zhai, Y.; Li, Y.; Song, D.; Pan, J. Gas Diffusion Characteristics and Size Effect in Coal Particles with Different Degrees of Metamorphism. *Energy Fuels* **2023**, *37* (3), 2030−2039.

(22) Wang, L.; Wang, B.; Zhu, J.; Liao, X.; Ni, S.; Shen, S. Experimental study on alleviating water-blocking effect and promoting coal gas desorption by gas wettability alteration. *J. Nat. Gas Sci. Eng.* **2022**, *108*, 104805.

(23) Yang, T.; Chen, P.; Li, B.; Nie, B.; Zhu, C.; Ye, Q. Potential safety evaluation method based on temperature variation during gas adsorption and desorption on coal surface. *Saf. Sci.* **2019**, *113*, 336−344.

(24) Du, Y.; Chen, X.; Li, L.; Wang, P. Characteristics of methane desorption and diffusion in coal within a negative pressure environment. *Fuel* **2018**, *217*, 111−121.

(25) Zhaoping, M.; Kun, Z.; Zhen, S. Difference analysis of methane diffusion properties between tectonic coal and primary coal. *Coal Geol. Explor.* **2022**, *50* (3), 102−109.

(26) Ma, D.; Gao, Z.; Chen, Y.; Zhang, H.; Shao, K.; Zhang, Z.; Wu, X.; Yang, F. Differences in methane adsorption and desorption characteristics of low, medium and high rank coal reservoirs at different temperatures. *Petroleum Reservoir Evaluation and Development* **2020**, *10* (04), 17−24. 38

(27) Guo, H.; Yuan, L.; Cheng, Y.; Wang, K.; Xu, C.; Zhou, A.; Zang, J.; Liu, J. Effect of moisture on the desorption and unsteady-state diffusion properties of gas in low-rank coal. *J. Nat. Gas Sci. Eng.* **2018**, *57*, 45−51.

(28) Zhao, J.; Xu, H.; Tang, D.; Mathews, J. P.; Li, S.; Tao, S. Coal seam porosity and fracture heterogeneity of macrolithotypes in the Hancheng Block, eastern margin, Ordos Basin, China. *Int. J. Coal Geol.* **2016**, *159*, 18−29.

(29) Peng, C.; Zou, C.; Yang, Y.; Zhang, G.; Wang, W. Fractal analysis of high rank coal from southeast Qinshui basin by using gas adsorption and mercury porosimetry. *J. Pet. Sci. Eng.* **2017**, *156*, 235−249.

(30) Liu, J.; Ren, B.; Wang, C. Pore structure characteristics of middle and low rank coals and their influence on gas desorption characteristics. *Coal Sci. Technol.* **2022**, *50* (12), 153−161.

(31) Hu, B.; Cheng, Y.; Wang, L. Study on porous structure and gas diffusion characteristics of primary structure coal and tectonic coal. *Coal Sci. Technol.* **2018**, *46* (03), 103−107.

(32) Wang, D.; Cheng, Y.; Yuan, L.; Wang, L.; Zhou, H. Experimental Study of Multiple Physical Properties of Tectonic Coal near a Minor Fault: Implications for Coal and Gas Outburst. *Energy Fuels* **2023**, *37* (8), 5878−5894.

(33) Zhao, W.; Cheng, Y.; Pan, Z.; Wang, K.; Liu, S. Gas diffusion in coal particles: A review of mathematical models and their applications. *Fuel* **2019**, *252*, 77−100.

(34) Zhao, F.; Deng, Z.; Wang, H.; Wang, Z.; Sun, P.; Yang, S. Influence of coal structure and macrolithotype of coal on coal adsorption and desorption of gas. *Coal Sci. Technol.* **2022**, *50* (12), 170−184.

(35) Ma, D.; Li, P.; Zhang, H.; Li, W.; Yang, F. Comparison on characteristics of adsorption/desorption of vitrain and durain in long-flame coal. *Nat. Gas Geosci.* **2017**, *28* (06), 852−862.

(36) Wei, H.; Fengyin, X.; Lei, Z.; Wei, Z.; Yanjun, M.; Qihu, L.; Yongchen, L.; Hongbo, F.; Hongya, W.; Shuangyuan, Z.; Wen, Z. Influence of coal lithotypes on adsorption/desorption characteristics in coal reservoirs and its practical significance: A case study in Baode Block. *Coal Geol. Explor.* **2022**, *50* (03), 110−118.

(37) Gao, Z.; Ma, D.; Chen, Y.; Zhang, H.; Zhang, L. Effect of water content on adsorption /desorption of methane of different macroscopic lithotypes. *Coal Sci. Technol.* **2020**, *48* (08), 97−105.

(38) Zhang, B.; Chen, Y. Particle size effect on pore structure characteristics of lignite determined via low-temperature nitrogen adsorption. *J. Nat. Gas Sci. Eng.* **2020**, *84*, 103633.

(39) Fu, X.; Qin, Y.; Ye, J.; Tang, S.; Zhang, Y. Desorption properties of some coal reservoirs and methane recovery recovery rate in china. *Coal Geol. Explor.* **2000**, *28* (02), 19−22.

(40) Van Niekerk, D.; Pugmire, R. J.; Solum, M. S.; Painter, P. C.; Mathews, J. P. Structural characterization of vitrinite-rich and inertinite-rich Permian-aged South African bituminous coals. *Int. J. Coal Geol.* **2008**, *76* (4), 290−300.

(41) Shi, G.; Han, C.; Wang, Y.; Wang, H. Experimental study on synergistic wetting of a coal dust with dust suppressant compounded

https://doi.org/10.1021/acsomega.3c04911
ACS Omega 2023, 8, 40417−40432

with noncationic surfactants and its mechanism analysis. *Powder Technol.* **2019**, *356*, 1077−1086.
(42) Ma, Z.; Chen, Y.; Ma, D.; Li, G.; Li, W.; Ji, Y.; Zheng, C.; Wang, L.; Wang, X. Pore Fractal Characteristics of Different Macro-Coal Components and Influence on Adsorption/Desorption: A Case Study in the Huanglong Jurassic Coalfield. *ACS Omega* **2022**, *7* (48), 43770−43783.
(43) Zhang, K.; Meng, Z.; Liu, S. Comparisons of Methane Adsorption/Desorption, Diffusion Behaviors on Intact Coals and Deformed Coals: Based on Experimental Analysis and Isosteric Heat of Adsorption. *Energy Fuels* **2021**, *35* (7), 5975−5987.
(44) Pan, Z. Modeling of coal swelling induced by water vapor adsorption. *Front. Chem. Sci. Eng.* **2012**, *6*, 94−103.
(45) Li, S.; Zhao, P.; Pan, H.; Xiao, P. Effect of moisture on adsorption of methane on coal. *J. Xi'an Univ. Eng. Sci. Technol.* **2011**, *31* (04), 379−382.
(46) Jiang, W.; Cui, Y.; Zhong, L.; Li, J.; Zhang, Q. Quantum chemical study on coal surface interacting with CH4 and H2O. *Nat. Gas Geosci.* **2007**, No. 04, 576−583.
(47) Zheng, C.; Ma, D.; Chen, Y.; Gao, Z.; Teng, J. Pore structure of different macroscopically distinguished components within low-rank coals and its methane desorption characteristics. *Fuel* **2021**, *293*, 120465.
(48) Nie, B. S.; Liu, X. F.; Guo, J. H.; Zhu, F. F. Effect of moisture on gas desorption and diffusion in coal mass. *J. China Univ. Min. Technol.* **2015**, *44* (05), 781−787.
(49) Wang, Z.; Su, W.; Tang, X.; Wu, J. Influence of water invasion on methane adsorption behavior in coal. *Int. J. Coal Geol.* **2018**, *197*, 74−83.
(50) Wang, M.; Wu, C. Study on Adsorption and Desorption Features of Coal Reservoir in Bide Santang Basin Under Multi Seam Condition. *Coal Eng.* **2014**, *46* (03), 118−121.
(51) Gamson, P. D.; Beamish, B. B.; Johnson, D. P. Coal microstructure and micropermeability and their effects on natural gas recovery. *Fuel* **1993**, *72* (1), 87−99.
(52) Hodot, B. B. *Outburst of Coal and Coalbed Gas*; Beijing China Coal Industry Press, 1966; pp 18−33. (Chinese Translation).
(53) Wang, B.; Qin, Y.; Shen, J.; Zhang, Q.; Wang, G. Pore structure characteristics of low- and medium-rank coals and their differential adsorption and desorption effects. *J. Pet. Sci. Eng.* **2018**, *165*, 1−12.
(54) Yao, Y.; Liu, D.; Tang, D.; Tang, S.; Huang, W.; Liu, Z.; Che, Y. Fractal characterization of seepage-pores of coals from China: An investigation on permeability of coals. *Comput. Geosci.* **2009**, *35* (6), 1159−1166.
(55) Li, Z.; Ren, T.; Li, X.; Cheng, Y.; He, X.; Lin, J.; Qiao, M.; Yang, X. Full-scale pore structure characterization of different rank coals and its impact on gas adsorption capacity: A theoretical model and experimental study. *Energy* **2023**, *277*, 127621.
(56) Wang, F.; Cheng, Y.; Lu, S.; Jin, K.; Zhao, W. Influence of Coalification on the Pore Characteristics of Middle−High Rank Coal. *Energy Fuels* **2014**, *28* (9), 5729−5736.
(57) Zhao, W.; Wang, K.; Wang, L.; Cheng, Y.; Dong, H.; Li, B.; Dai, L. Influence of matrix size and pore damage path on the size dependence of gas adsorption capacity of coal. *Fuel* **2021**, *283*, 119289.
(58) Peng, Z.; Deng, Z.; Feng, H.; Liu, S.; Li, Y. Multiscale Lattice Boltzmann Simulation of the Kinetics Process of Methane Desorption-Diffusion in Coal. *ACS Omega* **2021**, *6* (30), 19789−19798.
(59) Dang, Z.; Su, X.; Wang, X.; Wang, Q.; Hou, S. Gas desorption and diffusion characteristics in different rank coals under different pressure-drop conditions. *Geoenergy Sci. Eng.* **2023**, *221*, 111269.
(60) Chen, Y.; Zhang, B.; Qin, Y.; Li, Z.; Yang, Z.; Wu, C.; Cao, C. Differences in CH4 and C2H6 carbon isotopic compositions from open and closed pores in coal: Implications for understanding the two-stage δ13C shift during canister desorption. *Int. J. Coal Geol.* **2020**, *230*, 103586.
(61) Yan, J.; Feng, X.; Guo, Y.; Wang, W.; Wu, L.; Tan, Z. Desorption Effects and Laws of Multiscale Gas-Bearing Coal with Different Degrees of Metamorphism. *ACS Omega* **2021**, *6* (34), 22114−22125.
(62) Al-Omair, O. A. New Experimental Approach for Measuring Drainage and Spontaneous Imbibition Capillary Pressure. *Energy Fuels* **2009**, *23* (1), 260−271.

https://doi.org/10.1021/acsomega.3c04911
ACS Omega 2023, 8, 40417−40432